Journal of Alloys and Compounds 509 (2011) 1538–1543

Contents lists available at ScienceDirect

Journal of Alloys and Compounds

journal homepage: www.elsevier.com/locate/jallcom

Structural, morphological and optical properties of $Bi_{2-x}Sb_xSe_3$ thin films grown by electrodeposition

İlkay Şişman*, Mustafa Biçer

Department of Chemistry, Faculty of Arts and Sciences, Sakarya University, 54187 Sakarya, Turkey

ARTICLE INFO

Article history:
Received 14 August 2010
Received in revised form 13 October 2010
Accepted 27 October 2010
Available online 4 November 2010

Keywords:
$Bi_{2-x}Sb_xSe_3$
Alloy
Thin films
Electrodeposition
Band gap engineering

ABSTRACT

Ternary single-phase $Bi_{2-x}Sb_xSe_3$ alloy thin films were synthesized onto Au(1 1 1) substrates from an aqueous solution containing $Bi(NO_3)_3$, $SbCl_3$, and SeO_2 at room temperature for the first time via the electrodeposition technique. The electrodeposition of the thin films was studied using cyclic voltammetry, compositional, structural, optical measurements and surface morphology. It was found that the thin films with different stoichiometry can be obtained by controlling the electrolyte composition. The as-deposited films were crystallized in the preferential orientation along the (0 1 5) plane. The SEM investigations show that the film growth proceeds via nucleation, growth of film layer and formation of spherical particles on the film layer. The particle size and shape of $Bi_{2-x}Sb_xSe_3$ films could be changed by tuning the electrolyte composition. The optical absorption spectra suggest that the band gap of this alloy varied from 0.24 to 0.38 eV with increasing Sb content from $x = 0$ to $x = 0.2$.

1. Introduction

Thermoelectric materials useful for thermoelectric cooling at room temperature and below have attracted much attention recently because of their potential applications in superconductors and electronic apparatus. Thermoelectric materials are ranked by a figure of merit, ZT, which is defined as $ZT = S^2\sigma T/\kappa$, where S is the Seebeck coefficient, σ is the electrical conductivity, κ is the thermal conductivity, and T is the absolute temperature. The thermoelectric conversion efficiency of thermoelectric materials increases with the increase of ZT [1]. Bulk Bi_2Se_3 is a narrow direct band gap semiconductor of 0.24 eV [2]. Its thin films have potential application in thermoelectric, optical, photosensitive and IR photography devices [3]. Recently, it has been reported that thermoelectric properties of Bi_2Se_3 thin films can be improved by doping Sb [4].

In the formation of high-quality thermoelectric devices, several thin film formation methodologies are used, including molecular beam epitaxy (MBE), chemical vapor deposition (CVD) and sputtering [5–7]. In general, these methods are performed in vacuum and are thermal methods achieving compound formation by heating reactants and substrate. However, the electrochemical process is a particularly attractive route for processing thin films [8]. It offers the advantages of a low synthesis temperature, a simple and low cost preparation of thin or thick samples and a large area deposition on a laboratory scale [9].

Semiconductor thin films can be formed via surface-limited reactions by using atomic layer epitaxy (ALE). ALE involves the growth of compound thin films using surface-limited reactions to form single atomic layers of each element in a cycle. Electrochemical surface-limited reactions are generally referred to as underpotential deposition (UPD) [10]. The origin of the UPD phenomena is the free energy of formation of a surface compound between the depositing element and the substrate surface (electrode). UPD is a surface phenomenon that depends on the substrate structure, substrate physical–chemical characteristics, and deposit (adatom)–substrate interactions. As a result of the UPD process, which takes place at more positive potentials than the deposition equilibrium potential (Nernst potential), the electrode surface is partially or completely (up to an atomic layer) covered by a deposit. However, the overpotential deposition (OPD or bulk deposition) process is determined by electrode potential, deposit growth kinetics and mechanism (2D or 3D), electroactive species concentration, and deposit–substrate and deposit–deposit interactions. OPD takes place at more negative potentials than the Nernst equilibrium potential. Briefly, UPD may involve deposition onto substrate while OPD would involve deposition onto a substrate surface modified by an atomic layer, which was formed during the UPD process. Generally, deposits reach more than one atomic layer in the OPD regions [11]. Electrochemical atomic layer epitaxy (ECALE), developed by Gregory and Stickney, is the result of combining UPD with the principles of ALE to form a deposition cycle [10]. Atomic layers of a compound's component elements are deposited at underpotentials in a cycle to directly form a compound. However, this method is very time-consuming and produces a large amount of dilute

* Corresponding author. Tel.: +90 264 2956063; fax: +90 264 2955950.
E-mail address: isisman@sakarya.edu.tr (İ. Şişman).

0925-8388/$ – see front matter. Crown Copyright © 2010 Published by Elsevier B.V. All rights reserved.
doi:10.1016/j.jallcom.2010.10.165

wastewater because of the rinsing of the substrate after each deposition. Automated deposition systems by ECALE were developed to overcome these problems [12].

The electrodeposition of semiconductor thin films has been proposed to occur by the so-called induced codeposition mechanism, where both elements are deposited at the same time from the same solution [13]. Stoichiometry is maintained by having the more noble element as the limiting reagent. Codeposition holds great promise if greater control can be achieved. At present, the main points of control are solution composition and the deposition potential. Recently, we have reported codeposition of $Bi_2Te_{3-y}Se_y$, CdS, $Bi_{1-x}Sb_x$, and $Bi_{2-x}Sb_xTe_3$ under the conditions of UPD or OPD [14–16]. To the best of our knowledge, there is no report on the electrodeposition of $Bi_{2-x}Sb_xSe_3$ thin films. Herein, we report for the first time on the electrodeposition of $Bi_{2-x}Sb_xSe_3$ thin films under the conditions of OPD at room temperature. The structural, morphological and optical properties are presented and discussed.

2. Experimental

The $Bi_{2-x}Sb_xSe_3$ thin films were prepared on Au(1 1 1) substrates using an electrodeposition route. The cyclic voltammetry and electrodeposition experiments were carried out with a PAR model 2273 potentiostat/galvanostat connected to a three-electrode cell at room temperature (25 °C). The Au(1 1 1) working electrode, similar to a ball-shaped droplet, was (1 1 1)-oriented single-crystal gold (Alfa-Johnson Matthey, 99.999%) prepared as previously described by Hamelin [17]. In all electrochemical experiments, the reference electrode was an Ag/AgCl/3 M NaCl and a platinum wire was used as counter electrode.

The electrodeposition of the thin films was carried out in a bath containing 0.2 M $C_4H_6O_6$ (tartaric acid), 2.5 mM $Bi(NO_3)_3{\cdot}5H_2O$, 2.3 mM SeO_2 and varying the concentration of $SbCl_3$, all chemicals were AR grade. Tartaric acid was used as a complexing agent to improve the solubility of Sb in water through the formation of a Sb–tartaric complex. The pH of the solutions was adjusted to 1.0 ± 0.1 by using 0.1 M HNO_3 solution. Solutions were prepared with deionized water (i.e., >18 MΩ). Prior to each experiment, the solutions were purged with purified N_2 gas. Solutions were not stirred during all the electrochemical measurements and depositions. The deposition potential for $Bi_{2-x}Sb_xSe_3$ was determined from the cyclic voltammetry data. All samples in this study were electrodeposited at a potential of −0.21 V, with respect to the reference electrode, and at room temperature (25 °C). After each electrodeposition, the deposits were removed from the solution, and rinsed with deionized water and then dried in air at room temperature.

Characterization of the films was carried out with different techniques. The crystal structure of the films was investigated by an X-ray diffractometer (Rigaku, D-max 2200,) using Cu Kα radiation (λ = 1.54050 Å). Surface morphologies of the deposited films were observed with a scanning electron microscopy (SEM), JEOL, JSM-6060LV. The chemical compositions of the ternary thin films were determined by an energy-dispersive X-ray spectrometer (EDS) attached to the SEM. FT-IR absorbance spectra were recorded on a Shimadzu FT-IR-8000 series spectrophotometer in the wavelength range of 2500–6000 nm.

3. Results and discussion

3.1. Electrodeposition of ternary thin films

To determine the codeposition potentials for the elements, cyclic voltammetry experiments were performed on Au(1 1 1) substrates. The cyclic voltammogram of a Au(1 1 1) electrode in a solution of 2.5 mM $Bi(NO_3)_3{\cdot}5H_2O$ and 0.1 M HNO_3 is shown in Fig. 1a. The reductive peak C1 corresponding to the peak of Bi UPD and C2 is the OPD (bulk deposition) peak of Bi, where the oxidative stripping peaks of A2 and A1 correspond to C2 and C1, respectively. The voltammetric behavior of Bi on Au(1 1 1) is in good agreement with what has been reported in the literature [11]. The bulk deposition starts at about −0.01 V in this voltammogram. According to the cyclic voltammogram, if the potential of the electrode is kept constant at a potential within a range of 0.20 to −0.01 V (UPD region), an atomic layer of Bi is deposited at the electrode. When the electrode potential is shifted less potentials than −0.01 V (OPD region), more atomic layers of Bi is deposited on the substrate than UPD region. In comparison with Fig. 1a, the cyclic voltammogram for a Au(1 1 1) electrode in 2.3 mM SeO_2, and 0.1 M HNO_3 solution, is shown in Fig. 1b. Based on previous reports [18], the assignment of these voltammetric peaks (I–V) is as follows: underpotential deposition of Se (I–III), bulk deposition of selenium (IV), and formation of H_2Se (V) in a direct reduction by 6 electrons of Se^{4+}. In the reverse scan, the observed peak A is attributed to the Se oxidation.

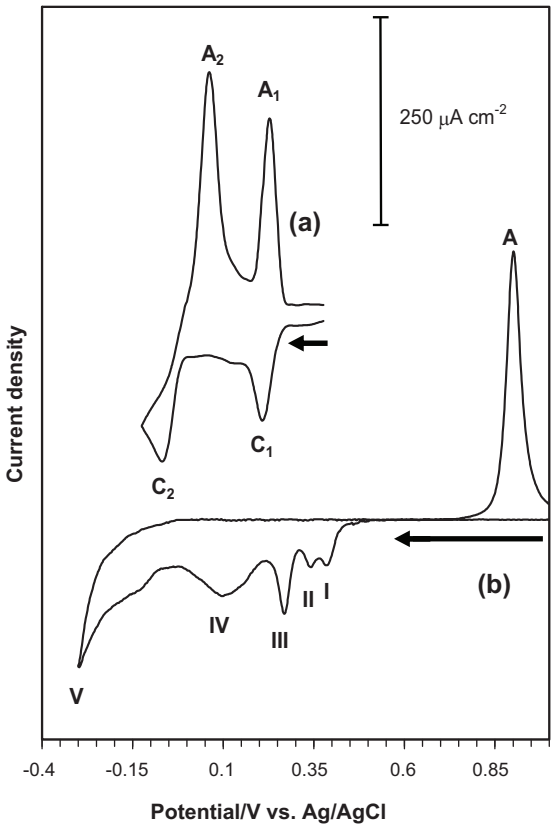

Fig. 1. Cyclic voltammograms of Au(1 1 1) electrode in 0.1 M HNO_3 solution containing: (a) 2.5 mM $Bi(NO_3)_3{\cdot}5H_2O$ and (b) 2.3 mM SeO_2. The scanning rate is 100 mV/s.

Fig. 2a displays the four voltammetric cycles of the Au(1 1 1) electrode in a solution of 2.5 mM $Bi(NO_3)_3{\cdot}5H_2O$ + 2.3 mM SeO_2 + 0.1 M HNO_3, each successive lower potential. If the electrode potential is scanned negatively to 0.25 V, two reduction peaks, labeled i and ii, and its stripping peak, labeled vii, are obtained. In comparison with their counterpart peaks, in Fig. 1b, these reduction peaks correspond to the peaks of Se UPD. When the potential of the working electrode is scanned negatively to 0.0 V, a relatively broad reduction peak (iii) and the stripping peak (vi) arise. Comparing with Fig. 1, the relatively broad reductive peak is considered to be the result of the Bi UPD peak as well as the Se OPD peak. The stripping peak (vi) corresponds to the oxidation of the Bi UPD. If the potential is scanned negatively to −0.20 V and reversed positively, the iv/v peak pair is observed. This peak pair is associated with Bi bulk deposition and oxidation. On the basis of the above results, if the electrode potential is kept constant at 0.0 V, which is suitable for the Bi UPD and Se OPD, Se-rich Bi_2Se_3 films will be deposited at the electrode surface. On the other hand, if the electrodeposition is performed from the same electrolyte at potential range of −0.03 V (peak iv) to more negative, which stands for the OPD region of each element, stoichiometric Bi_2Se_3 films may be deposited at the electrode.

In comparison with Fig. 2a, the cyclic voltammogram for a Au(1 1 1) electrode in 1 mM $SbCl_3$, 0.2 M $C_4H_6O_6$ and 0.1 M HNO_3 solution, is shown in Fig. 2b. In the range of the electrode potential between 0.60 and −0.25 V, the voltammogram is characterized by three cathodic features, labeled C_1–C_3, as well as by three anodic

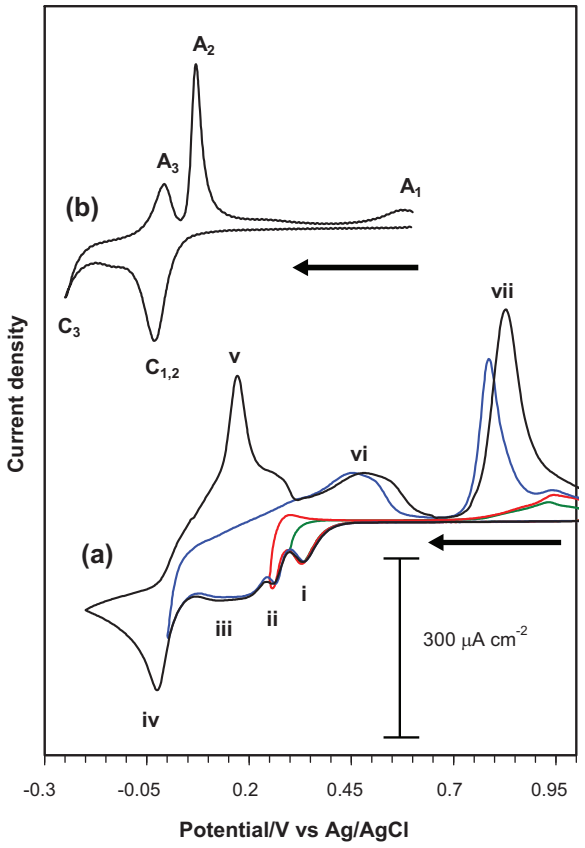

Fig. 2. Cyclic voltammograms of Au(1 1 1) electrode in the solutions containing 0.1 M HNO_3 and (a) 2.5 mM $Bi(NO_3)_3{\cdot}5H_2O$ and 2.3 mM SeO_2 and (b) 1 mM $SbCl_3$ and 0.2 M $C_4H_6O_6$. Scan rate: 100 mV/s.

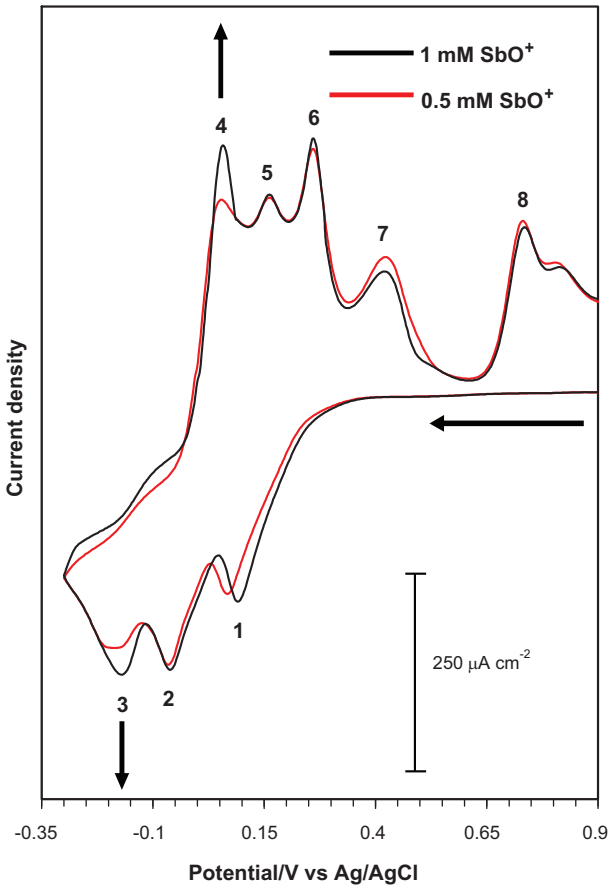

Fig. 3. Cyclic voltammograms of Au(1 1 1) electrode in the solution containing 2.5 mM $Bi(NO_3)_3{\cdot}5H_2O$, 2.3 mM SeO_2, 0.2 M $C_4H_6O_6$, 0.1 M HNO_3 and varying the concentration of $SbCl_3$. The scanning rate is 100 mV/s.

peaks, labeled A_3–A_1. The cathodic peak $C_{1,2}$ corresponds to the Sb UPD, while peaks A_1 and A_2 correspond to the anodic processes of $C_{1,2}$ [19]. Other peaks (C_3/A_3) correspond to the deposition and dissolution of bulk Sb in the OPD region. On the other hand, the bulk Sb deposition feature does not occur until about −0.20 V [16]. According to the cyclic voltammograms in Fig. 2a and b, if the electrodeposition is performed from the solution containing $Bi(NO_3)_3$, $SbCl_3$ and SeO_2 at potential range of −0.20 V to more negative, which stands for the OPD region of each element, ternary $Bi_{2-x}Sb_xSe_3$ films may be deposited at the electrode surface.

The cyclic voltammograms for a Au(1 1 1) electrode in 2.5 mM $Bi(NO_3)_3{\cdot}5H_2O$, 2.3 mM SeO_2, 0.2 M $C_4H_6O_6$, 0.1 M HNO_3 and varying the concentration of $SbCl_3$ electrolyte are shown in Fig. 3. In the range of the electrode potential between 0.90 and −0.30 V, the voltammogram is characterized by three cathodic features (1–3) as well as by five anodic peaks (4–8). The first reduction peak, labeled 1, appear at the same potential in comparison with their counterpart peak, labeled iii, in Bi–Se system (Fig. 2a). Subsequent reductive peak, labeled 2, is considered to be the result of the Bi OPD peak as well as the Sb UPD peak. Comparing with cyclic voltammogram of Sb in Fig. 2b, the last reductive peak (3) corresponds to the Sb OPD peak. In comparison with Figs. 1 and 2, the anodic peaks, labeled 4–8, correspond to the oxidative stripping peaks of Sb OPD, Sb UPD, Bi OPD, Bi UPD and Se, respectively. According to these cyclic voltammograms, if the electrodeposition is performed from $Bi(NO_3)_3$, SeO_2 and $SbCl_3$ at potential range of −0.20 V to more negative, which stands for OPD regions of each element, $Bi_{2-x}Sb_xSe_3$ films will be deposited at the electrode. As shown in Fig. 3, with increasing of the Sb ion concentration, the 3/4 peak pair (Sb OPD and its stripping) gets stronger whereas other peaks remain unchanged. It has been mentioned that the OPD is dependent on concentration. This indicated that the Sb content in Bi_2Se_3 can be changed by controlling the Sb ion concentration.

3.2. Structural and morphological properties of ternary thin films

In order to get more information about the reduction process in the Bi–Sb–Se ternary solution, the compositions of the films deposited at different Sb ion concentrations were evaluated by EDS, and the results are listed in Table 1. It can be seen that the atomic percentage of Sb in the films increases with the increase of Sb ion concentration. The deposit was also analyzed by XRD. Fig. 4 shows XRD spectrum of electrodeposited $Bi_{2-x}Sb_xSe_3$ ($x = 0.2$) thin films. The stick spectrum in the bottom of Fig. 4 is the XRD peaks of the reference hexagonal Bi_2Se_3 which have been assigned according to the standard JCPDS card (No. 33-0214). The XRD spectrum shows four peaks corresponding to (0 0 6), (0 1 5), (1 0 1 0), and (1 1 0) planes, respectively, and they all can be indexed as the hexagonal Bi_2Se_3. The diffraction peak observed at $2\theta = 38.22^\circ$ correspond to the Au(1 1 1) substrate. No additional impurity phases

Table 1
Atomic percentages and band gap energies of films.

Composition of solutions (mM)			Potential (V)	Atomic (%)			E_g (eV)
$Bi(NO_3)_3$	$SbCl_3$	SeO_2		Bi	Sb	Se	
2.5	–	2.3	−0.21	40.7	–	59.3	0.24
2.5	0.05	2.3	−0.21	39.4	0.5	60.1	0.28
2.5	0.2	2.3	−0.21	38.1	2.1	59.8	0.32
2.5	0.5	2.3	−0.21	36.2	4.3	59.5	0.38
2.5	1	2.3	−0.21	30.8	9.8	59.4	–

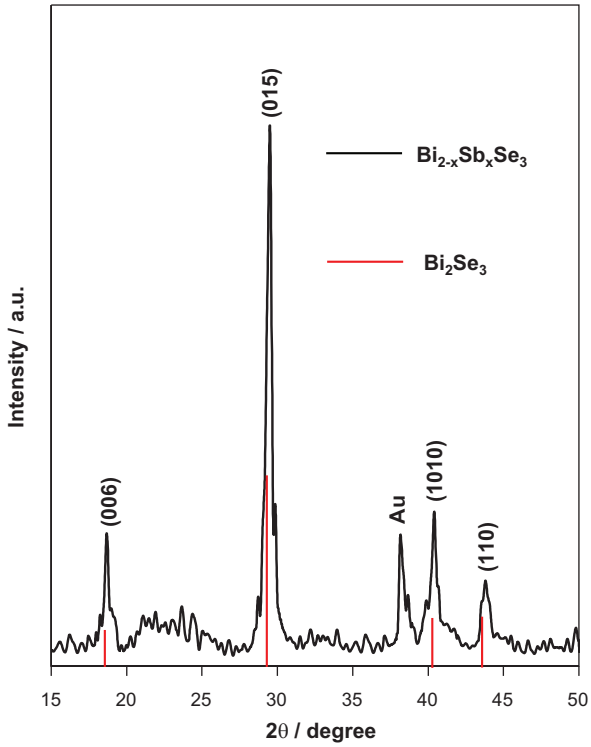

Fig. 4. XRD pattern of $Bi_{2-x}Sb_xSe_3$ ($x = 0.2$) thin film.

could be detected by XRD. It can be seen that the film has a preferred orientation along (0 1 5) diffraction plane. Compared with the reference hexagonal Bi_2Se_3, the diffraction peaks shift to larger angles with the incorporation of Sb along with the Bi. Since the Sb has lower atomic radius as compared to Bi, Sb can be easily incorporated into Bi_2Se_3, it causes a peak shift to larger angles. Consequently, XRD result suggests that the electrodeposition is able to induce ternary $Bi_{2-x}Sb_xSe_3$ alloys formation that may be described as

$$3H_2SeO_3 + (2-x)Bi^{3+} + xSbO^{+} + (12 + 2x)H^{+} + 18e^{-} \rightarrow Bi_{2-x}Sb_xSe_3 + (9+x)H_2O \quad (1)$$

Fig. 5a–c presents the SEM images of $Bi_{2-x}Sb_xSe_3$ ($x = 0.2$) thin films on Au(1 1 1) substrates electrodeposited at −0.21 V for 5, 45 and 150 min, respectively. It can be seen in Fig. 5a that the numerous well-separated nanoparticles about 60 nm in diameter were formed on the surface of the Au(1 1 1) electrode. When the deposition time is increased to 45 min, the entire surface is covered by spherical nanoparticles about 100 nm in diameter (Fig. 5b). We performed morphological experiments to investigate the $Bi_{2-x}Sb_xSe_3$ films forming at higher deposition times. When the deposition time is increased to 150 min, the new particles about 150 nm in diameter were formed on the former $Bi_{2-x}Sb_xSe_3$ surface (Fig. 5c). In contrast to the growth observed in Fig. 5a and b, these new particles are aggregated with each other. In other words, the subsequent growth is governed by the 3D growth. Fig. 6 shows the SEM images of $Bi_{2-x}Sb_xSe_3$ ($x = 0.02, 0.1, 0.3$) thin films electrodeposited at −0.21 V for 40 min. It can be easily observed that the particle size decreases with increasing Sb content. These results are consistent with the XRD result which also shows shifting of peaks to larger angles as a result of Sb doping indicating decrease of crystalline size.

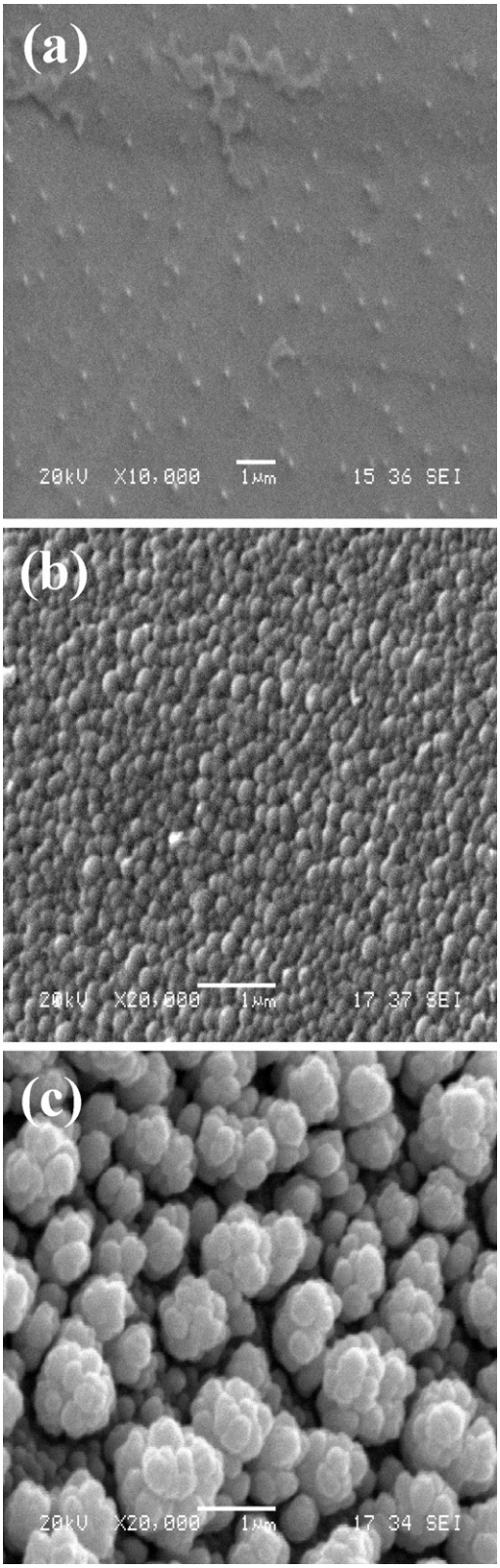

Fig. 5. SEM images of $Bi_{2-x}Sb_xSe_3$ ($x = 0.2$) thin films deposited at −0.21 V for various deposition times: (a) 5, (b) 45 and (d) 150 min.

3.3. Optical properties of ternary thin films

The FT-IR absorption spectra of as-prepared $Bi_{2-x}Sb_xSe_3$ thin films with different Sb substitutions are shown in Fig. 7a. It can be seen that the spectrum shifts towards higher energy values

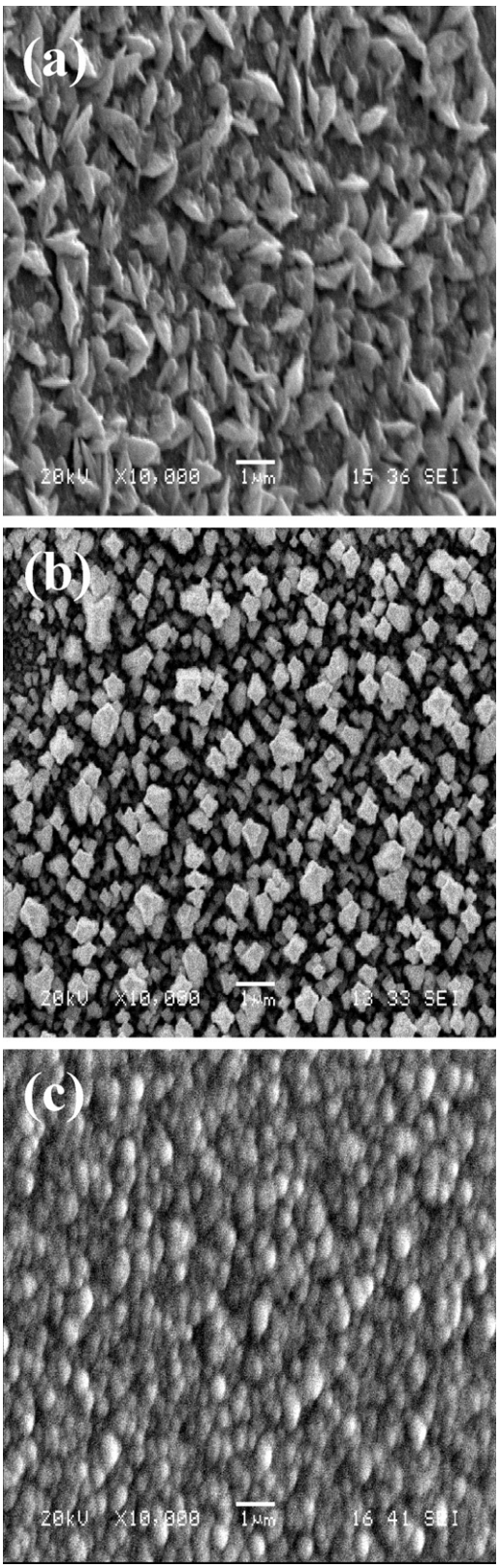

Fig. 6. SEM images for $Bi_{2-x}Sb_xSe_3$ films: (a) $x = 0.02$, (b) $x = 0.1$ and (c) $x = 0.3$.

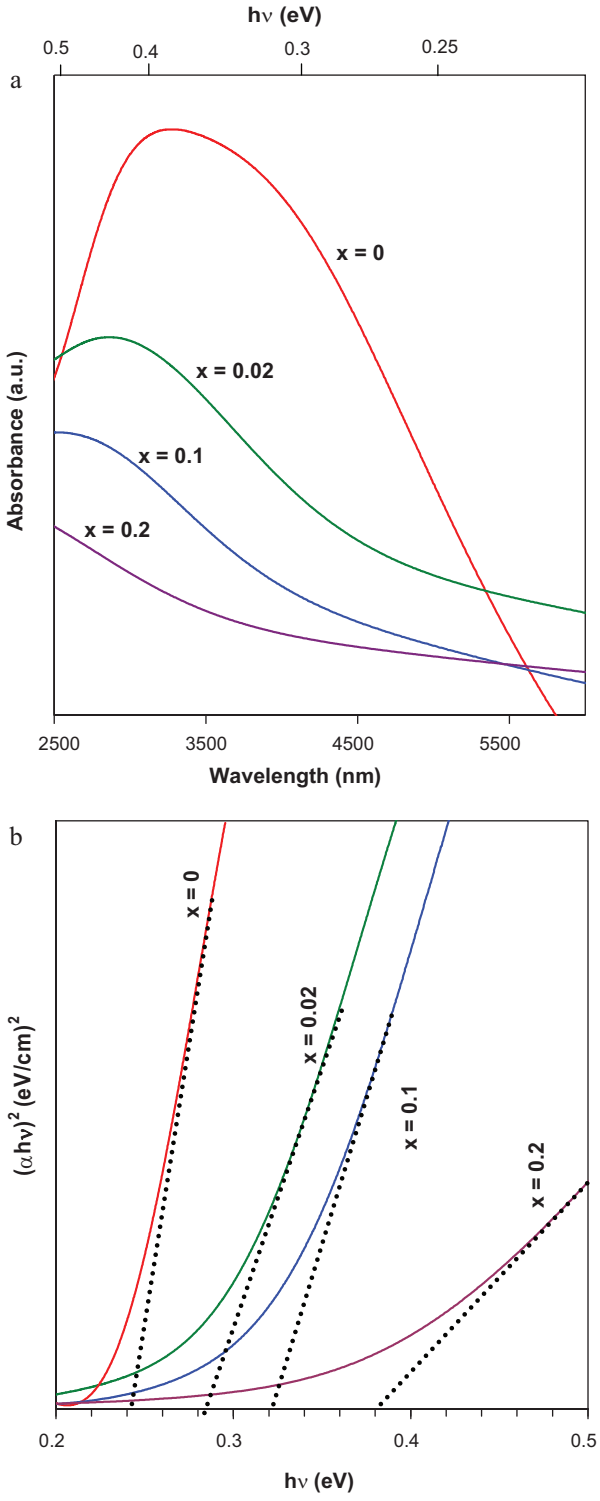

Fig. 7. (a) FT-IR spectra and (b) plots of $(\alpha h\nu)^2$ versus $h\nu$ of $Bi_{2-x}Sb_xSe_3$ films electrodeposited on Au(1 1 1) substrates at the potential of −0.21 V for different compositions.

with increasing Sb content (x) in the ternary thin films. From the absorbance data, the absorption coefficient α was calculated using Lambert law [20]

$$2.303A = \alpha d \tag{2}$$

where A is the optical absorbance and d is the film thickness. The film thickness was estimated using Faraday law [21], assuming 100% current efficiency,

$$d = \frac{QM}{\rho nFA} \tag{3}$$

where Q is the electric charge, M is the formula weight of $Bi_{2-x}Sb_xSe_3$, A is the deposition area, ρ is the density of $Bi_{2-x}Sb_xSe_3$,

n is the charge number and F is the Faraday constant. The density of $Bi_{2-x}Sb_xSe_3$ varies from 7.5 g/cm^3 ($x = 0$) to 5.81 g/cm^3 ($x = 2$). For films that were prepared in this study with $x \leq 0.2$, using 7.5 g/cm^3 does not introduce a thickness error exceeding 5%. The optical band gap of the thin film was determined by applying the Tauc and Menth's law [22] given by:

$$\alpha h\nu = A(h\nu - E_g)^m \quad (4)$$

where $h\nu$ is the photon energy, E_g is the band gap energy and A is a proportionality constant which is related to the effective masses associated with the bands. The value of m is equal to 1/2 for a direct band gap and 2 for indirect gap material. The absorption coefficient ($\alpha \geq 10^4$ cm^{-1}) is related to direct band transitions [23]. The value of absorption coefficient is found to be of the order of 10^4 cm^{-1} for all composition that supports the direct band gap nature of the semiconductor. The optical band gap was therefore determined by extrapolating the linear portion of the plot relating $(\alpha h\nu)^2$ versus $h\nu$ to $(\alpha h\nu)^2 = 0$ (Fig. 7b). In addition, the band gap energy values are given in Table 1. As shown in Fig. 7b, the band gap energy shifts from 0.24 to 0.38 eV as the composition of $Bi_{2-x}Sb_xSe_3$ film varied from $x = 0$ to $x = 0.2$. This clearly indicates a considerable increase in the band gap as a result of Sb-doping. Doping of Bi_2Se_3 with Sb is expected to alter the optical band gap between 0.24 (E_g of Bi_2Se_3) [2] and 1.2 eV (E_g of Sb_2Se_3) [24] in the resulting ternary $Bi_{2-x}Sb_xSe_3$ alloy. Thus, the observed modification in the band gap confirms the formation of ternary $Bi_{2-x}Sb_xSe_3$ alloy.

4. Conclusions

In this paper we reported for the first time the preparation of $Bi_{2-x}Sb_xSe_3$ thin films by electrodeposition technique. The electrochemistry and the codeposition potentials of Bi, Sb and Se were investigated by cyclic voltammetry. The electrodeposited thin films exhibit a hexagonal structure with a preferred orientation in the (0 1 5) direction. The morphologies of the films could be changed from leaf-like grains to spherical particles as the Sb content increases. The growth of the film proceeds via nucleation, growth of the smooth film layer and formation of aggregated spherical particles on the film layer. Optical band gap of films can be varied from 0.24 to 0.38 eV with increase in antimony concentration from $x = 0$–0.2 in the films.

Acknowledgement

Sakarya University is gratefully acknowledged for the financial support of this work.

References

[1] F. Li, W. Wang, Appl. Surf. Sci. 255 (2009) 4225.
[2] S.K. Mishra, S. Satpathy, O. Jepsen, J. Phys.: Condens. Mat. 9 (1997) 461.
[3] A. Jagminas, I. Valsiunas, G.P. Veronese, R. Juskenas, A. Rutavicius, J. Cryst. Growth 310 (2008) 428.
[4] N.S. Patil, A.M. Sargar, S.R. Mane, P.N. Bhosale, Mater. Chem. Phys. 115 (2009) 47.
[5] A. Boyer, E. Cisse, Mater. Sci. Eng. B: Solid 13 (1992) 103.
[6] R. Venkatasubramanian, T. Colpitts, E. Watko, M. Lamvik, N. El-Masry, J. Cryst. Growth 170 (1997) 817.
[7] A. Heinrich, H. Griessmann, G. Behr, K. Ivanenko, J. Schumann, H. Vinzelberg, Thin Solid Films 381 (2001) 287.
[8] M. Schlesinger, M. Paunovic, Modern Electroplating, 4th ed., Electrochemical Society Series, New York, 2000, pp. 868.
[9] D. Del Frari, S. Diliberto, N. Stein, C. Boulanger, J.M. Lecuire, J. Appl. Electrochem. 36 (2006) 449.
[10] B.W. Gregory, J.L. Stickney, J. Electroanal. Chem. 300 (1991) 543.
[11] C.A. Jeffrey, D.A. Harrington, S. Morin, Surf. Sci. 512 (2002) L367.
[12] B.H. Flowers, T.L. Wade, J.W. Garvey, M. Lay, U. Happek, J.L. Stickney, J. Electroanal. Chem. 524 (2002) 273.
[13] M.P.R. Panicker, M. Knaster, F.A. Kröger, J. Electrochem. Soc. 125 (1978) 566.
[14] H. Köse, M. Biçer, Ç. Tütünoğlu, A.O. Aydın, İ. Şişman, Electrochim. Acta 54 (2009) 1680.
[15] M. Biçer, A.O. Aydın, İ. Şişman, Electrochim. Acta 55 (2010) 3749.
[16] M. Biçer, H. Köse, İ. Şişman, J. Phys. Chem. C 114 (2010) 8256.
[17] A. Hamelin, in: B.E. Conway, R.E. White, J.O'M. Bockris (Eds.), Modern Aspects of Electrochemistry, vol. 16, Plenum Press, New York, 1985, p. 1.
[18] M.F. Cabral, V.A. Pedrosa, S.A.S. Machado, Electrochim. Acta 55 (2010) 1184.
[19] J.W. Yan, Q. Wu, W.H. Shang, B.W. Mao, Electrochem. Commun. 6 (2004) 843.
[20] A. Adachi, A. Kudo, T. Sakata, Bull. Chem. Soc. Jpn. 68 (1995) 3283.
[21] E.W. Bohannan, L.Y. Huang, F.S. Miller, M.G. Shumsky, J.A. Switzer, Langmuir 15 (1999) 813.
[22] J. Tauc, A. Menth, J. Non-Cryst. Solids 8/9 (1972) 569.
[23] K.R. Rajesh, C.S. Menon, Eur. Phys. J. B 47 (2005) 171.
[24] L.R. Gilbert, B. Van Pelt, C. Wood, J. Phys. Chem. Solids 35 (1974) 1629.